Rational design of dibenzo[*a,c*]phenazine-derived isomeric thermally activated delayed fluorescence luminophores for efficient orange-red organic light-emitting diodes

Hua Ye [a,c,*], Jiaji Yang [b], Kleitos Stavrou [c], Mengke Li [b], Fen Liu [d], Feiyun Li [a], Shi-Jian Su [b,**], Andrew P. Monkman [c,***]

[a] Department of Optoeletronic Engineering, Lishui University, Lishui 323000, China

[b] State Key Laboratory of Luminescent Materials and Devices and Institute of Polymer Optoelectronic Materials and Devices, South China University of Technology, Guangzhou 510640, China

[c] Department of Physics, Durham University, Durham DH1 3LE, U.K.

[d] Lishui Institute for Quality Inspection and Testing, Lishui 323000, China

ABSTRACT

It is an immense challenge to develop efficient long-wavelength (orange-to-red) thermally activated delayed fluorescence (TADF) materials due to the increasing nonradiative decay rates following the energy-gap law. Herein, two pairs of asymmetric isomers; DPyPzTPA and TPAPzDPy, and PyPzDTPA and DTPAPzPy based on electron-deficient moieties dibenzo[*a,c*]phenazine (Pz) and pyridine (Py) combined with electron-donor units of triphenylamine (TPA) were designed and synthesized. Their photophysical properties could be finely modulated by changing the position and number of Py groups as well as TPA fragments onto Pz cores. DPyPzTPA and DTPAPzPy possess much more rigidity and thus less geometry relaxation and non-radiative decay between ground states and excited states than those of PyPzDTPA and TPAPzDPy. Intriguingly, DPyPzTPA exhibits the highest relative photoluminescence

quantum yield (Φ_{PL}) and the fastest reverse intersystem crossing (rISC) rate among them owing to relatively stronger rigidity and spin-orbit coupling (SOC) interactions between the lowest singlet (S_1) and energetically close-lying excited triplet state and therefore, the device showed the highest maximum external quantum efficiency (EQE_{max}) of 16.6% (60.9 lm/W, 53.3 cd/A) with Commission Internationale de I'Eclairage (CIE) coordinates of (0.43, 0.55), peak wavelength 556 nm. In stark contrast, due to its lower rigidity and extremely weak delayed fluorescence (DF) characteristic and thus the much lower Φ_{PL}, TPAPzDPy-based devices are only half as efficient (30.8 lm/W, 27.5 cd/A, 8.3% EQE) despite the isomers possessing equal singlet-triplet energy gaps (ΔE_{ST}) of 0.43 eV. On the other hand, the device based on DTPAPzPy also demonstrated a strongly enhanced performance (59.1 lm/W, 52.7 cd/A, 16.1% EQE) than its isomer PyPzDTPA-based device (39.5 lm/W, 35.2 cd/A, 10.3% EQE). This work explicitly implicates that the asymmetric and isomeric molecular design is a potential strategy for promoting the development of highly efficient long-wavelength TADF materials.

Keywords: Dibenzo[*a,c*]phenazine, orange-red emitter, isomer, thermally activated delayed fluorescence, organic light-emitting diodes

*** Corresponding author**.

**** Corresponding author**.

***** Corresponding author**.

E-mail address: yehua@lsu.edu.cn (H. Ye), mssjsu@scut.edu.cn (S.-J. Su), a.p.monkman@durham.ac.uk (A.P. Monkman)

1. Introduction

Since the pioneering work of Adachi's group in 2012 [1], metal-free thermally activated delayed fluorescence (TADF) materials have triggered astonishing attention for their potential commercial organic light-emitting diodes (OLEDs) application due to the capability to achieve nearly 100% internal quantum efficiency (IQE) through fast reverse intersystem crossing (rISC) process [2-3]. In general, a high rate constant of rISC (k_{rISC}) is associated with low singlet-triplet energy gap (ΔE_{ST}) between the lowest singlet (S_1) and triplet (T_1) states which stems from the separation of the highest occupied molecular orbital (HOMO) and the lowest unoccupied molecular orbital (LUMO) [4-5]. However, according to Franck-Condon principle, such spatial separation typically leads to small spin-orbit coupling (SOC) and oscillator strength (f) values, and thus low photoluminescence quantum yield (Φ_{PL}) [6] but is overcome by the vibronic coupling mechanism to a second, energetically close triplet state [7-8]. Therefore, it is a challenge to simultaneously obtain low ΔE_{ST}, high rISC and high Φ_{PL}, which involves the use of a highly twisted donor-acceptor (D-A) system with strong charge transfer (CT) character excited states [9]. To date, some state-of-the-art blue and green TADF OLEDs with external quantum efficiency (EQE) beyond 30% have been reported on the basis of above-mentioned strategy or hyperfluorescence [10-20]. For instance, Kwon and coworkers developed quadrupolar D-A-D type of blue TADF emitter DBA-DTMCz and its hyperfluorescent devices exhibited the maximum EQE (EQE_{max}) of 43.9% and maximum current efficiency (CE_{max}) of 42.0 cd/A [12]. Nonetheless, as per the energy-gap laws, orange-red emitters are subject to more severe non-radiative decay than green and blue ones [21-22]. Consequently, highly efficient orange-red TADF OLEDs with EQE more than 30% are rarely reported [22-30].

To alleviate the detrimental non-radiative decay of orange-red luminophores, various strategies involving the utilizing of largely rigid and planar frameworks have been

invoked, such as dibenzo[*a*,*c*]phenazine [9, 28, 31-42], dibenzo[*a*,*j*]phenazine[43-44], dipyrido[3,2-*a*:2',3'-*c*]phenazine [22, 45-46], dibenzo[*a*,*c*]dipyrido[3,2-*h*:2',3'-*j*]phenazine [47], tetrabenzo[*a*,*c*]phenazine [48], dithieno[3,2-*a*:2',3'-*c*]phenazine [27, 49-50], azaacene [26], pyrazino[2,3-*f*][1,10]- phenanthroline-2,3-dicarbonitrile [29], quinoxaline [30, 51-52], dibenzo[*f*,*h*] quinoxaline [53-54], phenanthrene [55] and dibenzo[*f*,*h*]pyrrolo[3,4-*b*]quinoxaline- 10,12-dione [56]. As an example, in 2021, Zhao's group reported an orange-red device with EQE_{max} of 33.5%, maximum power efficiency (PE_{max}) of 85.8 lm/W and CE_{max} of 87.4 cd/A and Commission Internationale de I'Eclairage (CIE) coordinates of (0.49, 0.50) by employing dibenzo[*a*,*c*]phenazin-11- yl(phenyl)methanone as strong acceptor [28]. On the other hand, distinct substitution positions of the same groups also has tremendous implications on the photophysical properties and performance of emitters [23, 31, 35, 45-46, 50, 57-62]. For example, Li et al. constructed a pair of isomers by grafting two triphenylamine (TPA) donor moieties into two flanks of rigid planar acenaphtho[1,2-*b*]quinoxaline-9,10-dicarbonitrile acceptor core, the unique cruciform structure endows the molecule with relatively higher Φ_{PL} (95%) and smaller ΔE_{ST} (0.24 eV) than those of Y-shape counterpart (63%, 0.28 eV) and thereby realized excellent red OLEDs with EQE_{max} of 34.3% (64.8 lm/W, 54.7 cd/A) [23]. Previously, Kukhta et al. have unraveled that an additional intramolecular dipole interaction restricts ortho-D–A dihedral angle rotation in DMAC–BZN positional isomers [60]. And the interconversion of triplets via the rISC mechanism is promoted when parallel carbazole (Cz) and phenothiazine (PTZ) charge transfer states are allowed to interact [61]. Recently, we demonstrated that electronic interaction between the donating moieties alters the local excited triplet (^{3}LE) energy and thus also ΔE_{ST} and TADF performance [62].

In this contribution, we finely adjust the different substitution positions of identical donor/acceptor to control the photophysical properties of isomeric luminophores, and successfully designed and synthesized two pairs of asymmetric isomers based on the rigid and planar electron-withdrawing moiety of dibenzo[*a*,*c*]phenazine (Pz) (see Scheme 1), i.e., (11,12-di(pyridin-3-yl)dibenzo[*a*,*c*]phenazin-3-yl)-N,N-diphenylaniline (DPyPzTPA), 4,4'-(11-(pyridin-3-yl)dibenzo[*a*,*c*]phenazine-3,6-diyl)bis(N,N-diphenylaniline) (PyPzDTPA), 4-(3,6-di(pyridin-3-yl)dibenzo[*a*,*c*]phenazin-11-yl)-N,N-diphenylaniline (TPAPzDPy) and 4,4'-(3-(pyridin-3-yl)dibenzo[*a*,*c*]phenazine-11,12-diyl)bis(N,N-diphenylaniline) (DTPAPzPy). The meta-substituted pyridine (Py) rings were incorporated to boost the electron-transporting ability, the bulky TPA units were utilized as strong electron-rich segments and the robust steric hindrance to retard possible aggregation caused quenching (ACQ). It is envisioned that the two adjacent Py units or TPA fragments at 11/12 positions of Pz framework induces stronger intramolecular electronic interaction, larger molecular rigidity, decreased intramolecular rotation as well as probably smaller degree of geometry relaxation and thus reduced energy loss than those molecules with two substitutes in 3/6 positions. As anticipated, DPyPzTPA and DTPAPzPy possess much more rigidity and thus less geometry relaxation and non-radiative decay between ground states and excited states than those of PyPzDTPA and TPAPzDPy. Due to the relatively stronger rigidity and SOC interactions between the S_1 and energetically close-lying excited triplet state, DPyPzTPA exhibits the largest relative values of both Φ_{PL} and k_{rISC} among the four orange-red emitters. As a consequence, the corresponding device demonstrated the highest PE_{max} of 60.9 lm/W and CE_{max} of 53.3 cd/A with an EQE_{max} of 16.6% with CIE coordinates of (0.43, 0.55), peak wavelength 556 nm. On the contrary, owing to the lower rigidity and extremely weak delayed fluorescence (DF) behavior and thus the

much lower Φ_{PL}, TPAPzDPy-based devices are only half as efficient, (30.8 lm/W, 27.5 cd/A, 8.3% EQE) compared to DPyPzTPA even though both of the same (large) ΔE_{ST} value of 0.43 eV. In addition, the device based on DTPAPzPy also give significantly increased performance (59.1 lm/W, 52.7 cd/A, 16.1% EQE) than its analogue PyPzDTPA-based device (39.5 lm/W, 35.2 cd/A, 10.3% EQE). Our work demonstrates that the asymmetrical and isomeric molecular design is an effective strategy to promote the improvement of highly efficient long-wavelength TADF materials

2. Results and discussion

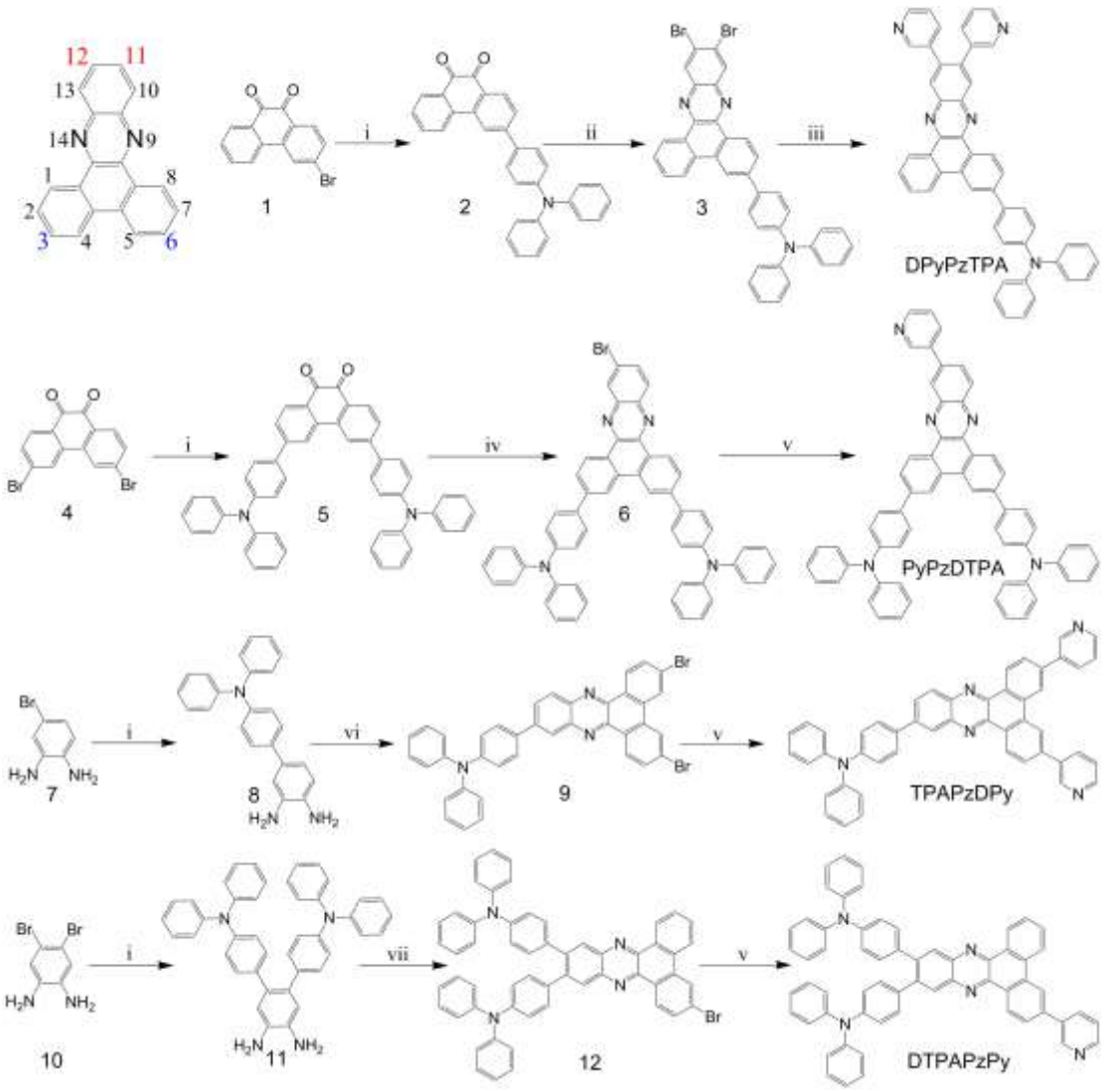

Scheme 1. Dibenzo[*a*,*c*]phenazine (Pz) core structure with position numbers and reaction conditions of materials: i: 4-(diphenylamino)phenyl boronic acid, 2M K_2CO_3, $Pd(PPh_3)_4$, 1,4-dioxane, 85 ^oC; ii: 4,5-dibromobenzene-1,2-diamine, acetic acid, 120 ^oC; iii: 3-(4,4,5,5-tetramethyl-1,3,2-dioxaborolan-2-yl)-pyridine, 2M K_2CO_3, $Pd(PPh_3)_4$, toluene, ethanol, 85 ^oC; iv: 4-bromobenzene-1,2-diamine, acetic acid, 120 ^oC; v: 3-pyridineboronic acid, 2M K_2CO_3, $Pd(PPh_3)_4$, toluene, ethanol, 85 ^oC; vi: 3,6-dibromophenanthrene-9,10-dione, acetic acid, 120 ^oC; vii: 3-bromophenanthrene-9,10-dione, acetic acid, 120 ^oC.

2.1.Synthesis and general characterizations

The synthesis routes of DPyPzTPA, PyPzDTPA, TPAPzDPy and DTPAPzPy are depicted in Scheme 1. The detailed experimental procedures can be found in the Supporting Information. We selected 3-bromophenanthrene-9,10-dione, 3,6-dibromophenanthrene-9,10-dione, 4-bromobenzene-1,2-diamine and 4,5-dibromobenzene-1,2-diamine as the starting materials, all of which were reacted with 4-(diphenylamino)phenyl boronic acid through typical palladium-catalyzed Suzuki cross-coupling reactions. Then, the key intermediate products were synthesized respectively from the condensation reactions. Finally, the target compounds were also obtained via Suzuki cross-coupling reactions between the intermediates and 3-pyridineboronic acid or 3-(4,4,5,5-Tetramethyl-1,3,2-dioxaborolan-2-yl)-pyridine. The chemical structures of materials were confirmed by ^1H NMR, ^{13}C NMR and high resolution mass spectra.

2.2. ***Theoretical calculations***

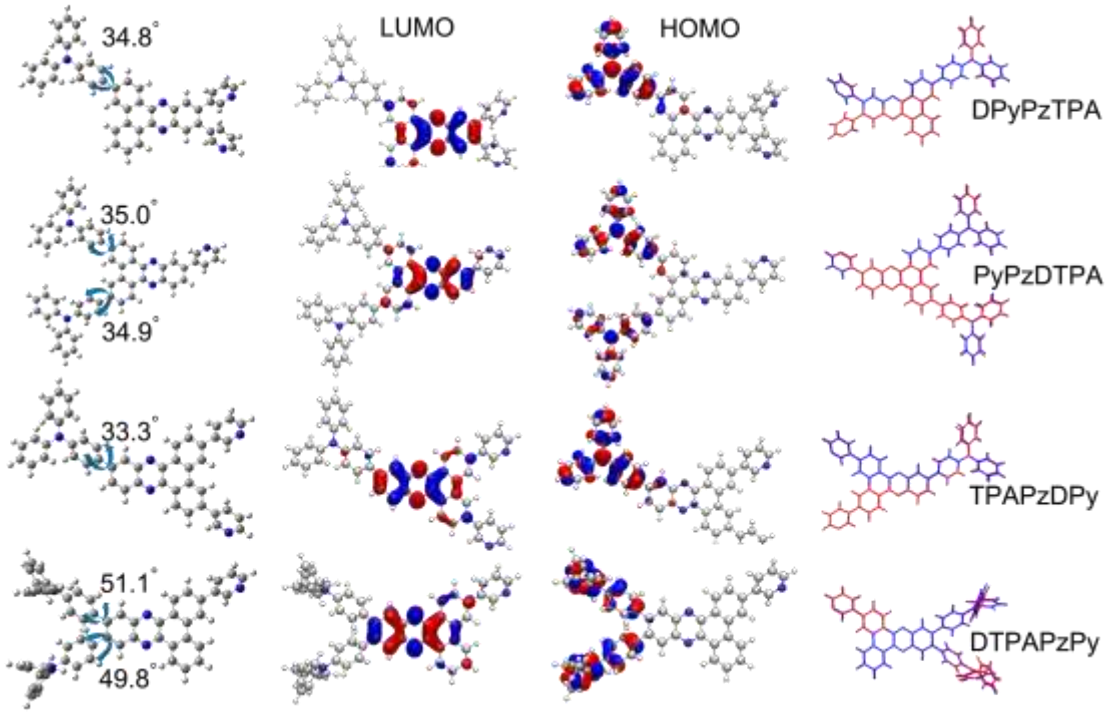

Fig. 1. Optimized ground state (S_0) geometries (left), calculated LUMO and HOMO space distributes (middle) and the comparison of the optimized structures of the S_0 (blue) with the S_1 (red) of the molecules (right).

To evaluate the electronic properties and molecular structure of these molecules, quantum chemical simulations were performed using the Gaussian 16 program package [63]. The ground state (S_0) geometries were optimized using B3LYP-D3/6-31G* theoretical level according to density functional theory (DFT). The excited state energies were calculated based on the optimized S_0 geometries using time-dependent density functional theory (TD-DFT) under the same theoretical level. As shown in Fig. 1, from the optimized ground-state geometries, it is abundantly clear that these molecules exhibit moderately twisted configuration with D-A dihedral angels 34.8° (DPyPzTPA), 35.0°/34.9° (PyPzDTPA), 33.3° (TPAPzDPy) and 51.1°/49.8° (DTPAPzPy), respectively. The largest torsion angel for DTPAPzPy could be originated from the steric repulsion of the two bulky TPA units in the 11/12 positions of Pz

framework. As expected, it is found that the LUMOs of all the molecules are mainly located over the skeleton of Pz acceptor, while the HOMO predominantly delocalized on TPA donor segments. Remarkably, Lower-lying LUMO energy levels (E_{LUMO}) of -2.40 eV and shallower-lying HOMO energy levels (E_{HOMO}) of -5.02 eV for DPyPzTPA are obtained compared to those of TPAPzDPy (-2.36 eV, -5.05 eV). Hence, DPyPzTPA displays much smaller band gap (E_g). For the other pair of isomer, the E_{LUMO} and E_{HOMO} of PyPzDTPA were deepened by 0.03 eV and 0.04 eV in comparison to those of DTPAPzPy, respectively, eventuating in their nearly identical E_g. Notably, the T_1 energy levels (E_{T1}) of DPyPzTPA is 2.10 eV, which is 0.09 eV higher than that of TPAPzDPy (2.01 eV), but their the S_1 energy levels (E_{S1}) are almost same. In terms of PyPzDTPA and DTPAPzPy, the phenomenon is found to be completely converse, indicating two electron-withdrawing groups at 3/6 positions of Pz is detrimental for retaining high E_{T1} because of the reinforced degree of molecular conjugation. Besides, more or bulky moieties at 11/12 positions of Pz is favorable to realizing low E_{S1} and small ΔE_{ST} due to the improvement of intramolecular electronic interaction and molecular rigidity. As consequence, relatively smaller ΔE_{ST} values and slightly larger oscillator strength (f) of DPyPzTPA (0.25 eV, 0.25) and DTPAPzPy (0.22 eV, 0.28) were calculated, suggesting the greater potential of TADF than their own counterparts (see Table 1). To evaluate the degree of geometry relaxation, the ground state and excited state geometries were optimized in the same theoretical level in gas phase (PBE1PBE/TZVP) (Fig. 1) according to DFT and TD-DFT, and the root-mean-square deviation (RMSD) values based on the comparisons of the optimized structures of S_0 and S_1 states were analyzed by visual molecular dynamics (VMD) software. It is found that the RMSD values of PyPzDTPA and TPAPzDPy are 0.23 and 0.21 Å, respectively, which are higher than those of DTPAPzPy (0.15 Å) and DPyPzTPA (0.14 Å) (see Table 1), indicating the

latter exhibit much larger rigidity, less geometry relaxation and non-radiative decay than the former [64-65]. Moreover, to access the SOC effect in these molecules, the SOC matrix element (SOCME) between different states were calculated (see Table S1). Note that the SOC matrix element (SOCME) between S_1 and energetically close-lying excited triplet state (T_n, n=1, 2, 3) of all the molecules are considerably tiny, implying the triplet excitons can not be efficiently up-converted to S_1 through rISC process.

Table 1

Physical properties of materials based on theoretical calculations.

Molecules	E_{HOMO} (eV)	E_{LUMO} (eV)	E_g [a] (eV)	E_{S1} (eV)	E_{T1} (eV)	E_{T2} (eV)	E_{T3} (eV)	ΔE_{ST} [b] (eV)	*Oscillator strengths* (*f*)	RMSD [c] (Å)
DPyPzTPA	-5.02	-2.40	2.62	2.35	2.10	2.35	2.67	0.25	0.25	0.14
PyPzDTPA	-4.97	-2.29	2.68	2.41	2.11	2.19	2.50	0.30	0.14	0.23
TPAPzDPy	-5.05	-2.36	2.69	2.36	2.01	2.41	2.66	0.35	0.35	0.21
DTPAPzPy	-4.93	-2.26	2.67	2.34	2.12	2.18	2.53	0.22	0.28	0.15

[a] $E_g = |E_{HOMO}| - |E_{LUMO}|$

[b] $\Delta E_{ST} = E_{S1} - E_{T1}$

[c] Root-mean-square deviation (RMSD) of the comparison of the optimized structures of the S_0 with the S_1 of the molecules

2.3. Thermal and Electrochemical properties

Table 2

Summary of the physical properties of materials.

Molecules	λ_{em} [a] (nm)	E_{HOMO} /E_{LUMO} [b] (eV)	E_g^{opt} [c] (eV)	T_d/T_g [d] (°C)	Φ_{PL}/Φ_P F/Φ_{DF} [e] (%)	E_{S1}/ E_{T1}/ ΔE_{ST} [f] (eV)	k_{PF}/ k_{DF} [g] (×10^8 S^{-1})/ (×10^3 S^{-1})	τ_{PF}/τ_{DF} [h] (ns)/ (ms)	k_r^S/ k_{nr}^S [i] (×10^8 S^{-1})/ (×10^8 S^{-1})	k_{ISC}/ k_{rISC} [j] (×10^7 S^{-1})/ (×10^3 S^{-1})
DPyPzTPA	536/590/ 548	-5.01 /- 2.73	2.28	465 /-	59.1/5 0.9/8.2	2.64/2.2 1/0.43	2.22/1.28	4.50/0. 78	1.13/0.78	3.10/ 1.48
PyPzDTPA	528/582/ 550	-5.02 /- 2.64	2.38	262 /-	27.5/2 4.1/3.4	2.62/2.1 8/0.44	2.32/0.78	4.31/1. 29	0.56/1.48	2.84/ 0.90
TPAPzDPy	543/590/ 562	-5.05 /- 2.72	2.33	313 /135	27.6/2 7.6/-	2.58/2.1 5/0.43	4.69/-	2.13/-	1.30/3.39	0.001 4/-
DTPAPzPy	535/574/ 553	-5.04 /- 2.71	2.33	487 /140	50.7/4 2.6/8.1	2.47/2.1 6/0.31	2.36/0.18	4.23/5. 54	1.01/0.97	3.81/ 0.21

[a] PL maximum measured in 10^{-6} M toluene solution/neat films/10 wt% doped CBP film at RT.

[b] E_{HOMO} calculated from the onsets of the oxidation curves, $E_{LUMO} = |E_{HOMO}| - |E_g^{opt}|$.

[c] Optical band gap measured in neat film.

[d] Measured by TGA/DSC under N_2.

[e] Photoluminescence quantum yield measured in 10 wt% doped CBP film under N_2, the prompt

fluorescence and delayed fluorescence Φ_{PL} under N_2.

[f] Estimated from the onset values of fluorescence/phosphorescence spectra in 1 wt% doped zeonex film at 80 K, $\Delta E_{ST} = E_{S1} - E_{T1}$.

[g] Rate constants of prompt and delayed fluorescence measured in 10 wt% doped CBP film at RT.

[h] Prompt fluorescence/delayed fluorescence lifetime measured in 10 wt% doped CBP film at RT.

[i] Rate constants of radiation and non-radiation transition process.

[j] Rate constants of ISC and rISC transition process.

As depicted in Table 2 and Fig. S1 (a), DPyPzTPA and DTPAPzPy exhibit much better thermal stability with 5% weight-loss temperatures (T_d) of 465 °C and 487 °C than TPAPzDPy (313 °C) and PyPzDTPA (262 °C) owing to the two adjacent Py units or TPA fragments at 11/12 positions of Pz framework leads to much stronger intramolecular electronic interaction, enhanced steric hindrance effect and larger molecular rigidity than those molecules with two substitutes in 3/6 positions which has been mentioned in theoretical calculations previously. It could be seen from the DSC spectra (Fig. S1 (b)) that TPAPzDPy and DTPAPzPy disclose high glass transition temperatures (T_g) of 135 °C and 140 °C, respectively. By comparison, no T_g were observed for DPyPzTPA and PyPzDTPA, implying that the four compounds could form thermally durable thin-films with morphological stability, which is beneficial to the stable and long-lifespan devices.

To estimate the HOMO and LUMO levels of the orange-red luminogens, cyclic voltammetry (CV) was carried out. Under the same experimental conditions, the redox potential ($E_{1/2}$) of ferrocene/ferrocenium (Fc/Fc^+) was determined to be 0.52 V to the Ag/Ag^+ reference electrode (Fig.S2). Note that the absolute energy level of redox

potential of Fc/Fc^+ to vacuum is -4.8 eV, consequently, the E_{HOMO} are calculated according to the following equations: E_{HOMO} = -e (E_{ox} + 4.28) (eV), where E_{ox} is the onset oxidation potential, E_{HOMO} of all the materials are ranging from -5.01 eV to -5.05 eV (Table 2 and Fig. S2), such shallow E_{HOMO} is conductive to the holes from the anode effectively be injected into the emitting layer (EML). The E_{LUMO} of the materials are obtained from the difference between their E_{HOMO} and the optical band gap (E_g^{opt}). E_g^{opt} is estimated from the wavelengths corresponding to their absorption edges in the long wavelength direction in the thin film state (Table 2). The lower lying E_{LUMO} are obtained through the introduction of Pz backbone with fortissimo electron-withdrawing capability. Additionally, the two Py rings at 3/6 or 11/12 positions of Pz endow the comparatively deeper E_{LUMO} to DPyPzTPA and TPAPzDPy compared to PyPzDTPA and DTPAPzPy, which is in good consistency with theoretical calculations.

2.4. Photophysical properties

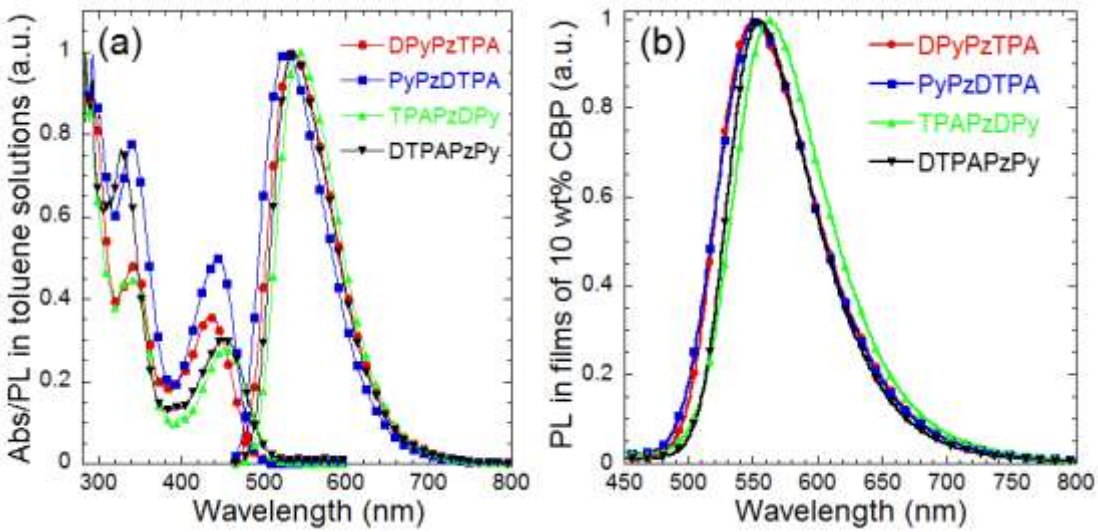

Fig. 2. UV-visible absorption and PL spectra in toluene solution (a) and PL spectra in 10 wt% doped CBP film (b).

In dilute toluene solution (Fig.2 (a)), the intense absorption bands below 390 nm can be assigned to the π-π* and n-π* transitions. The relatively weak absorption ranging from 390 nm to 520 nm could be ascribed to the intramolecular charge transfer (ICT) transition from TPA to Pz/Py moieties. In the neat film state, due to molecular interactions, the low-energy absorption minimum red-shifted to exceeding 600 nm (see Fig. S3(a)).

As shown in Fig. 2 (a), the PL spectra of the four emitters in dilute toluene solution exhibit the maximum emission peaks in the range of 528 nm to 543 nm. In stark contrast, due to the intense aggregation of the quasi planar molecules, the emission bands of the in neat films are significantly red-shifted to 590, 582, 590 and 574 nm, (DPyPzTPA, PyPzDTPA, TPAPzDPy and DTPAPzPy) respectively. (see Table 2 and Fig. S3(b)). To alleviate this aggregation behavior, we doped the compounds into the popular host matrix of 4,4'-bis(carbazol-9-yl)biphenyl (CBP) with doping ratio of 10 wt%. As anticipated, the broad and structureless emission of these doped films slightly bathochromic shifts, but by only about 20 nm, compared with those in toluene solution (Fig. 2 (b)). The Φ_{PL} of the materials in thin solid films are listed in Table 2. It is worth noting that the highest Φ_{PL} value of DPyPzTPA (59.1%) is more than twice that of PyPzDTPA (27.5%) and TPAPzDPy (27.6%), whereas DTPAPzPy also has comparable Φ_{PL} of 50.7%. The much higher Φ_{PL} of DPyPzTPA and DTPAPzPy probably due to they possess much larger rigidity and thus less geometry relaxation and non-radiative decay between ground states and excited states than PyPzDTPA and TPAPzDPy, which accounts for their higher device EQE to large degree.

In order to investigate the ICT property of these molecules, four solvents with distinctive polarity (methylcyclohexane (MCH), toluene (Tol), dichloromethane (DCM), acetone (Ace)) were chosen to conduct the solvatochromic experiments. It can

be seen from Fig. S4, all four compounds show strong positive solvatochromism indicative of the CT character of their lowest excited states [49]. Surprisingly, with increasing the polarity from MCH to Ace, the absorption intensity of DPyPzTPA and TPAPzDPy increases. Furthermore, the PL peaks of DPyPzTPA, PyPzDTPA, TPAPzDPy and DTPAPzPy appreciably red-shift by about 269, 266, 211, and 216 nm, respectively, indicative of strong solvent dipole relaxation of the excited state dipole moment. In order to obtain the accurate ΔE_{ST} values, fluorescence and phosphorescence spectra of the materials in films of zeonex (cyclic olefin polymer, a nonpolar soft polymer matrix) at 1 wt% at 80 K under vacuum were measured [66]. Herein, zeonex was used as host matrix because of its large free volume comparable to a (highly viscous) MCH solution [67]. Since zeonex is an inert environment, thus, the fluorescence spectra can be compared with the ones in MCH solutions. In both cases, the fluorescence spectra are structured (Figure S4, S5). This phenomenon is expected in non-polar environments because the CT state is not stabilized, and all molecules exhibit stronger local character. As shown in Fig. S5, the well-defined vibrational phosphorescence spectra shape of DPyPzTPA, PyPzDTPA, TPAPzDPy and DTPAPzPy reveals their T_1 states are all ^{3}LE state [68], which manifests the probability of rISC processes from T_1 (^{3}LE) to S_1 (^{1}CT) since their rISC channels involve a change in orbital type [65, 69]. E_{S1} and E_{T1} were estimated based on their onset values of fluorescence and phosphorescence spectra, thus, the ΔE_{ST} of DPyPzTPA, PyPzDTPA, TPAPzDPy and DTPAPzPy were calculated to be 0.43, 0.44, 0.43 and 0.31 eV, respectively (see Table 2). Such large ΔE_{ST} values suggests only weak or no TADF should occur in these four

emitters.

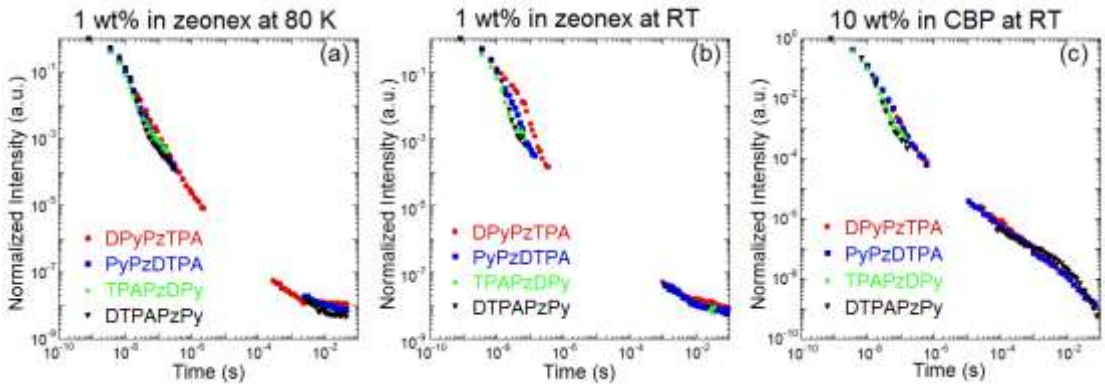

Fig.3 Time-resolved PL decays of materials doped in 1 wt% zeonex (a: 80K; b: RT) and 10 wt% CBP (c: RT). Data points not plotted indicate no emission. Excitation at 355 nm.

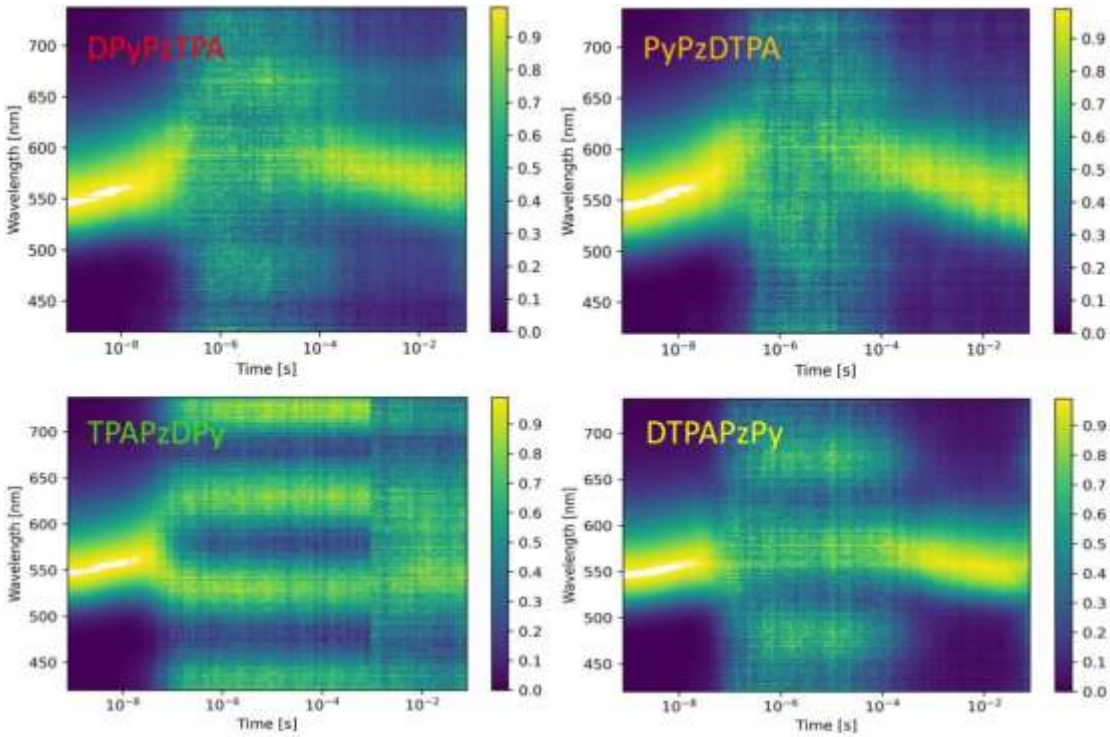

Fig.4 The contour plots of PL in films of 10 wt% in CBP over time at RT. Banded region indicates the noise floor of the detection system, i.e. no measurable signal.

To verify our aforementioned scenario, oxygen-sensitive PL spectra were first

measured at RT. As shown in Fig. S6, the fluorescence intensity of DPyPzTPA and DTPAPzPy have more intense emission in nitrogen conditions compared to those in air, indicative of some triplet exciton harvesting contributing to the emission in comparison to the weak increase seen in PyPzDTPA and TPAPzDPy. To substantiate if this arises from a TADF channel, transient PL decay measurements were proceeded on the materials doped in 1 wt% zeonex and 10 wt% CBP (Fig.3-4 and Fig. S7). It is noteworthy that in zeonex, which provides an environment similar to the solution state [70], the delayed emission is only observed at long times and is redshifted, indicative of phosphorescence. As the temperature increased from 80 K to RT, the delayed contribution of DPyPzTPA decreased, while for DTPAPzPy, it was completely quenched, the absence of their emission at the delayed regime > 0.1 ms again is ascribed to the phosphorescence emission since the slopes of the decay get closer to zero at 80 K [67]. For PyPzDTPA, the slightly enhanced emission was observed, regarding TPAPzDPy, only a little emission was found as illustrated in Fig. 3 (b), the faint improvement of the delayed components by elevating the temperature support their considerably weak TADF features. The heat maps, Fig 3 and S7 do indicate redshifted emission at 10 ns -50 ns which we ascribe to aggregate state emission from the more planar molecules. However, a large enhancement of DF was observed in all except TPAPzDPy when the four materials were doped in the universal rigid host of CBP (with reinforced polarizability) and elevated concentration, 10 wt % (see Fig. 3 (c)). As shown in Table 2 and Fig.S8-S11, the prompt and delayed lifetimes are 4.50 ns/0.78 ms (DPyPzTPA), 4.31 ns/1.29 ms (PyPzDTPA) and 4.23 ns/5.54 ms (DTPAPzPy),

respectively. The DF emission in this case is not red shifted and come from the same state as the prompt emission indicative of a triplet harvesting mechanism. We then calculated the kinetic parameters to gain deep insights into the exciton dynamics according to reported methods [40, 71]. As summarized in Table 2, the radiation rate constants of the lowest singlet state (k_r^S) of DPyPzTPA and DTPAPzPy are larger than their corresponding nonradiative decay rates (k_{nr}^S), suggesting the deactivation process of the S_1 is dominated by the radiative transitions [72]. Additionally, the highest ratio of k_r^S/k_{nr}^S was noticed for DPyPzTPA, which means the most efficient radiative decay process [72]. On the contrary, both of TPAPzDPy and PyPzDTPA exhibit much lower ratio of k_r^S/k_{nr}^S which indicative of unsatisfactory radiation transitions. These results further testified that DPyPzTPA and DTPAPzPy possess much more rigidity and thus less geometry relaxation than TPAPzDPy and PyPzDTPA. Impressively, DPyPzTPA is found to have the highest effective k_{rISC} (1.48×10^3 s^{-1}), demonstrating the triplet excitons could up-convert to singlet ones more efficiently than other three analogs. On the contrary, TPAPzDPy exhibited extremely weak DF in 10 wt% CBP which cannot be observed. We then measured the time-resolved behaviour of the four emitters in a high dielectric/polarizability host DPEPO (bis[2-(diphenylphosphino)phenyl]ether oxide), and observed that there is a delayed fluorescence component for TPAPzDPy (see Fig. S12). Based on this result and an extremely weak signal in the delayed region of the 10 wt% CBP film, we conclude that TPAPzDPy has DF which is the worst in the four molecules of the series but cannot be easily observed. The less rigidity of molecular skeleton of TPAPzDPy leads to its much lower ratio of k_r^S/k_{nr}^S and thus the severely

non-radiative decay process despite it shows the relatively higher SOC value. Overall, the weak SOC interactions between S_1 and energetically close excited triplet states as well as the large ΔE_{ST} values accounts for their relatively small k_{rISC} values and long TADF lifetime [73]. As shown in Table 2, the values of k_{rISC} of DPyPzTPA (1.48×10^3 s^{-1}) is much higher than those of PyPzDTPA (0.90×10^3 s^{-1}) and DTPAPzPy (0.21×10^3 s^{-1}) although DTPAPzPy exhibits the smallest $\Delta E_{ST.}$ This results could be explained by the relatively stronger SOC interactions between S_1 and energetically close-lying excited triplet state (i.e., T_2 and T_3) for DPyPzTPA as revealed by theoretical calculations (see Table S1) [68, 73]. To corroborate that no other processes participate the time-resolved PL of DPyPzTPA, the variation of the DF integrated intensity with excitation dose is an important criterion to establish the intramolecular origin of the DF [74], thus, laser excitation intensity measurements were performed over two time ranges of 1.5-100 μs and 10-30 ms, as illustrated in Fig.S13, all of which are linear in the entire regime with the slopes < 1, ruling out the triplet-triplet annihilation (TTA) mechanism and validating its TADF behavior [66-67, 70, 74-75].

3.5. Electroluminescence

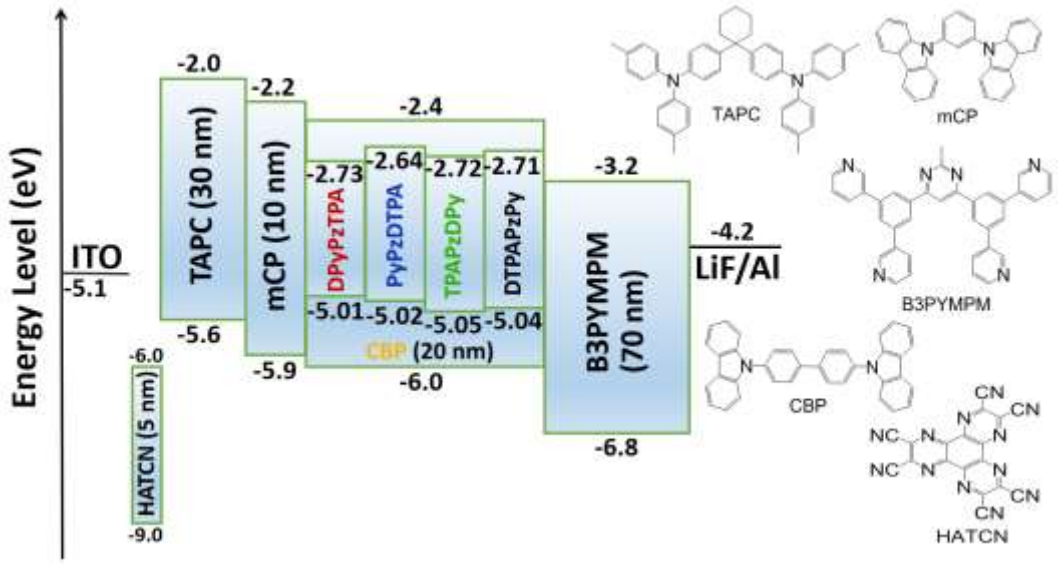

Fig. 5. The energy level diagram of the devices and the molecular structures.

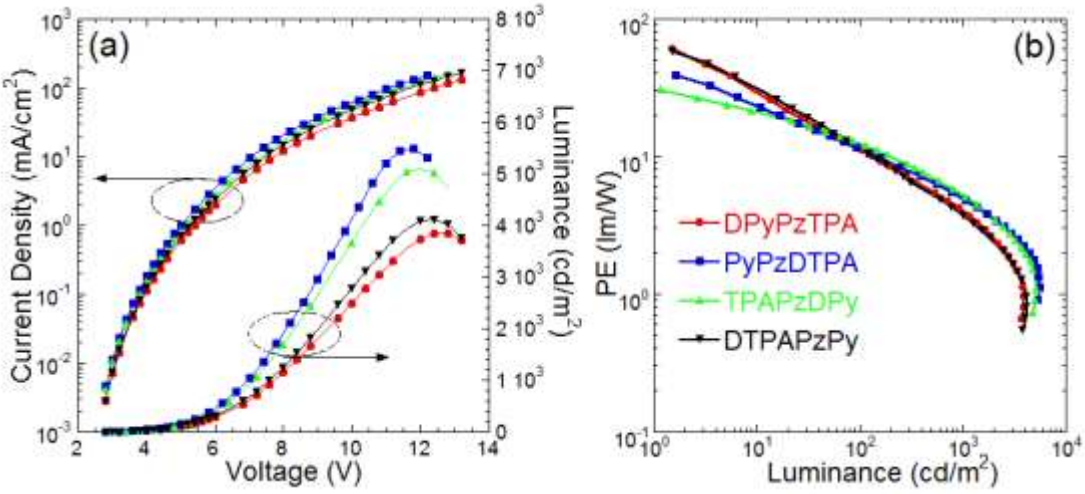

Fig. 6. Current density and luminance versus voltage of the devices (a) and power efficiency versus luminance of the devices (b).

To investigate the potential OLEDs application of these materials, various devices of ITO / HATCN (5 nm) / TAPC (30 nm) / mCP (10 nm) / EML (20 nm) / B3PYMPM (70 nm) / LiF (1 nm) / Al (150 nm) were fabricated (see Fig. 5), where HATCN

(2,3,6,7,10,11-hexacyano-1,4,5,8,9,12-hexaazatriphenylene) is hole-injection layer (HIL), TAPC (1,1-bis(4-di-p-tolylaminophenyl)cyclohexane) is hole-transporting layer (HTL), mCP (m-bis(N-carbazolyl)benzene) is exciton blocking layer, B3PYMPM (4,6-bis(3,5-di-3-pyridylphenyl)2-methylpyrimidine) is electron-transporting layer (ETL), LiF (lithium fluoride) is electron-injection layer (EIL), CBP doped with different concentrations of emitter as EML. We observed that slightly red-shift of emission peaks with the increasing concentrations due to the enhanced intermolecular interaction and polarity in EML (Table S2-S5). For DPyPzTPA, as shown in Table S2, when the concentration rose from 5% to 10%, a bit improved performance was found. However, the device showed significantly decreased efficiency as doping concentration further increased to 15% onwards which can be assigned to the gradually aggravated ACQ effect because of its quasi planar molecular skeleton. Since almost all the devices represented the highest EQE_{max} at the doping concentration of 10 wt%, to this end, we explored their electroluminescent properties at this same concentration for better comparison. From Fig. 6(a) and Table 3, it can be seen that all the devices exhibited the low turn-on voltage of 2.8 V which means their excellent charge carrier transport capacity. As illustrated in Fig. 6(b), Fig. 7 and Table 3, thanks to the largest Φ_{PL} and k_{rISC}, the device based on DPyPzTPA disclosed the best PE_{max}, CE_{max} and EQE_{max} of 60.9 lm/W, 53.3 cd/A and 16.6%, respectively. In stark contrast, TPAPzDPy-based device only achieved nearly half efficiency (30.8 lm/W, 27.5 cd/A, 8.3%) compared to its brethren of DPyPzTPA. The EQE_{max} value of 8.3% for TPAPzDPy-based fluorescent device might is arising from extremely weak DF property and much lower Φ_{PL} of TPAPzDPy. Concurrently, in terms of the other pair of isomers, the DTPAPzPy-based device also manifested much more intensified performance (59.1 lm/W, 52.7 cd/A, 16.1%) than those of PyPzDTPA's device (39.5 lm/W, 35.2 cd/A, 10.3%) benefiting

from the relatively higher Φ_{PL}. The EQE roll-off (difference between EQE_{max} and EQE at 1000 cd/m^2) is 13.5%, 7.3%, 4.9% and 13.8% for DTPAPzPy, PyPzDTPA, TPAPzDPy and DPyPzTPA, respectively. This shows that the roll-off is much smaller in TPAPzDPy. As above-mentioned, we stated that some DF is possible to occur but will be very weak and inefficient, thus a small contribution from this will affect the device's roll-off. In comparison to the TPAPzDPy and PyPzDTPA-based devices, the devices based on DPyPzTPA and DTPAPzPy also demonstrated noticeable efficiency roll-off stemming from the long TADF lifetimes of these materials and less ideal rISC process with relatively small k_{rISC} values which probably induced frustrating triplet exciton accumulations at high brightness and thus severe quenching processes such as TTA, singlet-triplet annihilation (STA) and triplet-polaron quenching (TPQ) during operation [24, 76-77].

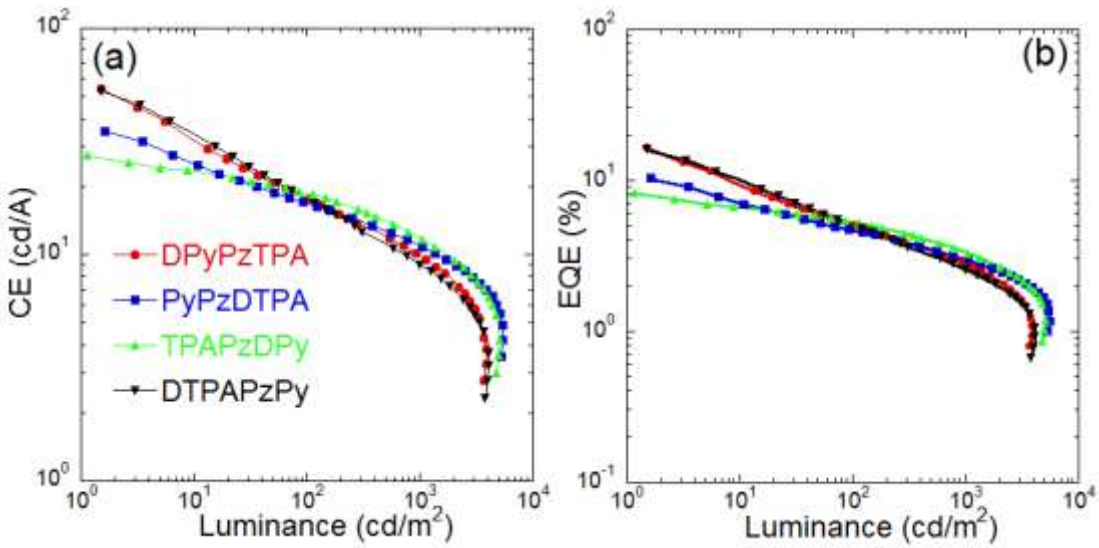

Fig. 7. Current efficiency versus luminance of the devices (a) and external quantum efficiency versus luminance of the devices (b).

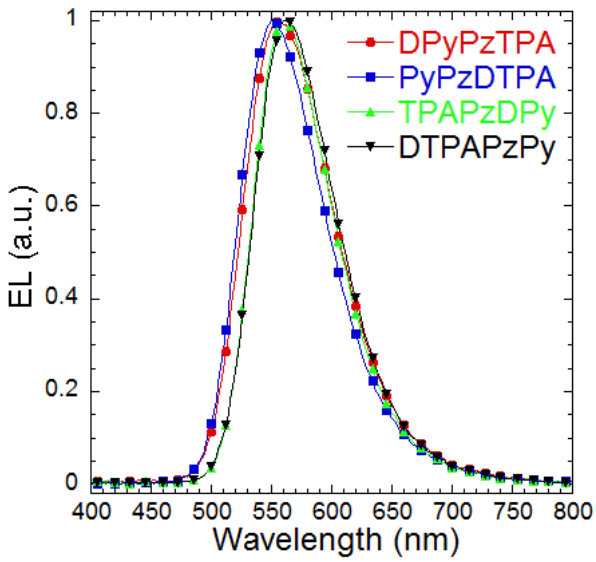

Fig. 8. Electroluminescence spectrum of the devices.

The EL spectra of all the devices displayed typically orange-red emission bands (Fig. 8). The EL peaks of DPyPzTPA, PyPzDTPA, TPAPzDPy and DTPAPzPy-based devices are located at 556, 550, 560, and 562 nm, respectively (Table 3), which are in good consistency with their PL peaks (Table 2), corroborating that the EL emissions were purely originated from the TADF materials.

Table 3

Summary of the electroluminescent performance of the devices based on ITO / HATCN (5 nm) / TAPC (30 nm) / mCP (10 nm) / CBP: 10% emitter (20 nm) / B3PYMPM (70 nm) / LiF (1 nm) / Al (150 nm).

Emitter	V_{on}[a] (V)	L_{max} (cd/m^2)	PE (lm/W)	CE (cd/A)	EQE (%)	*Peak* (nm)	*CIE* (*x*, *y*)
DPyPzTPA	2.8	3855	60.9[b]	53.3[b]	16.6[b]/5.1[c]/2.8[d]	556	(0.43,0.55)

PyPzDTPA	2.8	5484	39.5[b]	35.2[b]	10.3[b]/4.7[c]/3.0[d]	550	(0.41,0.56)
TPAPzDPy	2.8	5101	30.8[b]	27.5[b]	8.3[b]/5.3[c]/3.4[d]	560	(0.45,0.54)
DTPAPzPy	2.8	4113	59.1[b]	52.7[b]	16.1[b]/5.1[c]/2.6[d]	562	(0.46,0.53)

[a] Turn-on voltage at the luminance of 1 cd/m^2.

[b] maximum.

[c] at 100 cd/m^2.

[d] at 1000 cd/m^2.

4. Conclusion

In summary, we have designed and synthesized four orange-red emitters named DPyPzTPA and TPAPzDPy, PyPzDTPA and DTPAPzPy with slightly twisted A'-A-D or D-A-A' structures. Their photophysical properties could be controlled through altering the position and number of substituted groups. Among them, DPyPzTPA and DTPAPzPy exhibit much more rigidity and thus less geometry relaxation and non-radiative decay between ground states and excited states than those of PyPzDTPA and TPAPzDPy. Thanks to the relatively stronger rigidity and SOC interactions between the S_1 and energetically close-lying excited triplet state, DPyPzTPA represents the relatively highest Φ_{PL} and the fastest rISC process, accordingly, the device based on DPyPzTPA exhibited the highest PE_{max} of 60.9 lm/W and CE_{max} of 53.3 cd/A with a EQE_{max} of 16.6% and CIE coordinates of (0.43, 0.55). By contrast, the TPAPzDPy-based devices only presented half efficiency (30.8 lm/W, 27.5 cd/A, 8.3%) owing to its lower rigidity, extremely weak DF feature and much lower Φ_{PL}. Meanwhile, the device based on DTPAPzPy also demonstrated the enormously boosted performance (59.1 lm/W, 52.7 cd/A, 16.1%) than its counterpart PyPzDTPA-based device (39.5 lm/W,

35.2 cd/A, 10.3%). Our work implies that the asymmetrical and isomeric molecules is a potential strategy of designing highly efficient long-wavelength TADF materials.

CRediT authorship contribution statement

Hua Ye: Investigation, Validation, Conceptualization, Data curation, Writing - original draft. **Jiaji Yang:** Investigation, Validation, Data curation. **Kleitos Stavrou:** Investigation, Validation, Data curation, Isualization, Writing - review & editing. **Mengke Li:** Software. **Fen Liu:** Investigation. **Feiyun Li:** Investigation. **Shi-Jian Su:** Conceptualization, Resources. **Andrew P. Monkman:** Resources, Writing - review & editing.

Declaration of competing interest

The authors declare that they have no known competing financial interests or personal relationships that could have appeared to influence the work reported in this paper.

Data availability

Data will be made available on request.

Acknowledgements

This work was financially supported by the Basic Public Welfare Research Program of Zhejiang Province (LGG18E030003) and China Scholarship Council (202008330262).

Appendix A. Supplementary data

Supplementary data to this article can be found online at

References

[1] Uoyama H, Goushi K, Shizu K, Nomura H, Adachi C. Highly efficient organic light-emitting diodes from delayed fluorescence. Nature, 2012;492(7428):234–40. https://doi.org/10.1038/nature11687.

[2] Dias FB, Bourdakos KN, Jankus V, Moss KC, Kamtekar KT, Bhalla V, Santos J, Bryce MR, Monkman AP. Triplet harvesting with 100% efficiency by way of thermally activated delayed fluorescence in charge transfer OLED emitters. Adv Mater, 2013;25(27):3707–14. https://doi.org/10.1002/adma.201300753.

[3] Goushi K, Yoshida K, Sato K, Adachi C. Organic light-emitting diodes employing efficient reverse intersystem crossing for triplet-to-singlet state conversion. Nature Photon 2012;6(4):253–8. https://doi.org/10.1038/nphoton.2012.31.

[4] Zhang Q, Li B, Huang S, Nomura H, Tanaka H, Adachi C. Efficient blue organic light-emitting diodes employing thermally activated delayed fluorescence. Nature Photon 2014;8(4):326–32. https://doi.org/10.1038/nphoton.2014.12.

[5] Tao Y, Yuan K, Chen T, Xu P, Li H, Chen R, Zheng C, Zhang L, Huang W. Thermally activated delayed fluorescence materials towards the breakthrough of organoelectronics. Adv Mater 2014;26(47):7931–58. https://doi.org/10.1002/adma. 201402532.

[6] Liu Y, Li C, Ren Z, Yan S, Bryce MR. All-organic thermally activated delayed fluorescence materials for organic light-emitting diodes. Nat Rev Mater 2018;3:18020. https://doi.org/10.1038/natrevmats.2018.20.

[7] Gibson J, Monkman AP, Penfold TJ.The importance of vibronic coupling for

efficient reverse intersystem crossing in thermally activated delayed fluorescence molecules. ChemPhysChem 2016;17(19):2956–61. https://doi.org/10.1002/cphc.201600662.

[8] Etherington MK, Gibson J, Higginbotham HF, Penfold TJ, Monkman AP. Revealing the spin–vibronic coupling mechanism of thermally activated delayed fluorescence. Nat Commun 2016;7(1):13680. https://doi.org/10.1038/ncomms13680.

[9] Jiang D, Sasabe H, Arai H, Nakao K, Kumada K, Kido J. Extremely high power efficiency solution-processed orange-red TADF OLEDs via a synergistic strategy of molecular and device engineering. Adv Opt Mater 2022;10(6):2102774. https://doi.org/10.1002/adom.202102774.

[10] Hua T, Miao J, Xia H, Huang Z, Cao X, Li N, Yang C. Sulfone-incorporated multi-resonance TADF emitter for high-performance narrowband blue OLEDs with EQE of 32%. Adv Funct Mater 2022;32(31):2201032. https://doi.org/10.1002/adfm.202201032.

[11] Lv X, Miao J, Liu M, Peng Q, Zhong C, Hu Y, Cao X, Wu H, Yang Y, Zhou C, Ma J, Zou Y, Yang C. Extending the π-skeleton of multi-resonance TADF materials towards high-efficiency narrowband deep-blue emission. Angew Chem Int Ed 2022;61(29):e202201588. https://doi.org/10.1002/anie.202201588.

[12] Lee H, Braveenth R, Muruganantham S, Jeon CY, Lee HS, Kwon JH. Efficient pure blue hyperfluorescence devices utilizing quadrupolar donor-acceptor-donor type of thermally activated delayed fluorescence sensitizers. Nat Commun 2023;14:419. https://doi.org/10.1038/s41467-023-35926-1.

[13] Jiang P, Miao J, Cao X, Xia H, Pan K, Hua T, Lv X, Huang Z, Zou Y, Yang C. Quenching-resistant multiresonance TADF emitter realizes 40% external

544 quantum efficiency in narrowband electroluminescence at high doping level. Adv
545 Mater 2022;34(3):2106954. https://doi.org/10.1002/adma.202106954.
546 [14] Chen Y, Zhang D, Zhang Y, Zeng X, Huang T, Liu Z, Li G, Duan L. Approaching
547 nearly 40% external quantum efficiency in organic light emitting diodes utilizing
548 a green thermally activated delayed fluorescence emitter with an extended linear
549 donor-acceptor-donor structure. Adv Mater 2021;33(44):2103293.
550 https://doi.org/10.1002/adma.202103293.
551 [15] Wang Q, Xu Y, Yang T, Xue J, Wang Y. Precise functionalization of a multiple-
552 resonance framework: constructing narrowband organic electroluminescent
553 materials with external quantum efficiency over 40%. Adv Mater
554 2023;35(3):2205166. https://doi.org/10.1002/adma.202205166.
555 [16] Konidena RK, Naveen KR. Boron-based narrowband multiresonance delayed
556 fluorescent emitters for organic light-emitting diodes. Adv Photonics Res
557 2022;3(11):2200201. https://doi.org/10.1002/adpr.202200201.
558 [17] Han J, Chen Y, Li N, Huang Z, Yang C. Versatile boron-based thermally activated
559 delayed fluorescence materials for organic light-emitting diodes. Aggregate
560 2022;3:e182. https://doi.org/10.1002/agt2.182.
561 [18] Kim HJ, Yasuda T. Narrowband emissive thermally activated delayed
562 fluorescence materials. Adv Opt Mater 2022;10(22):2201714.
563 https://doi.org/10.1002/adom.202201714.
564 [19] Cai X, Su SJ. Marching toward highly efficient, pure-blue, and stable thermally
565 activated delayed fluorescent organic light-emitting diodes. Adv Funct Mater
566 2018;28(43):1802558. https://doi.org/10.1002/adfm.201802558.
567 [20] Shi YZ, Wu H, Wang K, Yu J, Ou XM, Zhang XH. Recent progress in thermally
568 activated delayed fluorescence emitters for nondoped organic light-emitting

diodes. Chem Sci 2022;13(13): 3625–51. https://doi.org/10.1039/D1SC07180G.

[21] Kim JH, Yun JH, Lee JY. Recent progress of highly efficient red and near-infrared thermally activated delayed fluorescent emitters. Adv Opt Mater 2018;6(18):1800255. https://doi.org/10.1002/adom.201800255.

[22] Zhang HY, Yang HY, Zhang M, Lin H, Tao SL, Zheng CJ, Zhang XH. A novel orange-red thermally activated delayed fluorescence emitter with high molecular rigidity and planarity realizing 32.5% external quantum efficiency in organic light-emitting diodes. Mater Horiz 2022;9(9):2425−32. https://doi.org/10.1039/D2MH00639A.

[23] Yang T, Liang J, Cui Y, Li Z, Peng X, Su SJ, Wang Y, Li C. Achieving 34.3% external quantum efficiency for red thermally activated delayed fluorescence organic light-emitting diode by molecular isomer engineering. Adv Opt Mater 2023;11(1):2201191. https://doi.org/10.1002/adom.202201191.

[24] Cheng YC, Fan XC, Huang F, Xiong X, Yu J, Wang K, Lee CS, Zhang XH. A highly twisted carbazole-fused DABNA derivative as an orange-red TADF emitter for OLEDs with nearly 40% EQE. Angew Chem Int Ed 2022;61(47):e202212575. https://doi.org/10.1002/anie.202212575.

[25] Zeng X, Huang YH, Gong S, Li P, Lee WK, Xiao X, Zhang Y, Zhong C, Wu CC, Yang C. An unsymmetrical thermally activated delayed fluorescence emitter enables orange-red electroluminescence with 31.7% external quantum efficiency. Mater Horiz 2021;8(8):2286−92. https://doi.org/10.1039/D1MH00613D.

[26] Wang XJ, Liu H, Zhang K, Yang D, Pan ZH, Wang CK, Fung MK, Ma D, Fan J. Using azaacene as an acceptor unit to construct an ultraefficient red fluorophore with an EQE over 40%. Mater Horiz 2023;10(3):938−44. https://doi.org/10.1039/D2MH01322C.

[27] Yang CZ, Pan ZH, Zhang K, Tai JW, Wang CK, Ding L, Fung MK, Fan J. Intramolecular charge transfer effect for highly efficient deep red and near infrared thermally activated delayed fluorescence. Mater Horiz 2023;10(3):945−51. https://doi.org/10.1039/D2MH01015A.

[28] Jiang R, Wu X, Liu H, Guo J, Zou D, Zhao Z, Tang BZ. High-performance orange–red organic light-emitting diodes with external quantum efficiencies reaching 33.5% based on carbonyl-containing delayed fluorescence molecules. Adv Sci 2022;9(3):2104435. https://doi.org/10.1002/advs.202104435.

[29] Cai Z, Wu X, Liu H, Guo J, Yang D, Ma D, Zhao Z, Tang BZ. Realizing record-high electroluminescence efficiency of 31.5% for red thermally activated delayed fluorescence molecules. Angew Chem Int Ed 2021;60(44):23635–40. https://doi.org/10.1002/anie.202111172.

[30] Li Z, Yang D, Han C, Zhao B, Wang H, Man Y, Ma P, Chang P, Ma D, Xu H. Optimizing charge transfer and out-coupling of a quasi-planar deep-red TADF emitter: towards rec.2020 gamut and external quantum efficiency beyond 30%. Angew Chem Int Ed 2021;60(27):14846–51. https://doi.org/10.1002/anie.202103070.

[31] Tan JH, Jin JM, Chen WC, Cao C, Wang R, Zhu ZL, Huo Y, Lee CS. The role of balancing carrier transport in realizing an efficient orange-red thermally activated delayed-fluorescence organic light-emitting diode. ACS Appl Mater Interfaces 2022;14(47):53120−8. https://doi.org/10.1021/acsami.2c17492.

[32] Zhang YL, Ran Q, Wang Q, Liu Y, Hänisch C, Reineke S, Fan J, Liao LS. High-efficiency red organic light-emitting diodes with external quantum efficiency close to 30% based on a novel thermally activated delayed fluorescence emitter. Adv Mater 2019;31(42):1902368. https://doi.org/10.1002/adma.201902368.

[33] Xie FM, Wu P, Zou SJ, Li YQ, Cheng T, Xie M, Tang JX, Zhao X. Efficient orange–red delayed fluorescence organic light-emitting diodes with external quantum efficiency over 26%. Adv Electron Mater 2020;6(1):1900843. https://doi.org/10.1002/aelm.201900843.

[34] Huang FX, Li HZ, Xie FM, Zeng XY, Li YQ, Hu YY, Tang JX, Zhao X. Efficient orange-red thermally activated delayed fluorescence material containing a cyano group, Dyes Pigments 2021;195:109731. https://doi.org/10.1016/j.dyepig.2021.109731.

[35] Kothavale S, Lim J, Lee JY. Rational design of CN substituted dibenzo[a,c]phenazine acceptor for color tuning of thermally activated delayed fluorescent emitters. Chem Eng J 2022;431:134216. https://doi.org/10.1016/j.cej.2021.134216.

[36] Jiang C, Miao J, Zhang D, Wen Z, Yang C, Li K. Acceptor-donor-acceptor π-stacking boosts intramolecular through-space charge transfer towards efficient red TADF and high-performance OLEDs. Research 2022:9892802. https://doi.org/10.34133/2022/9892802.

[37] Liang J , Li C , Cui Y , Li Z , Wang J , Wang Y. Rational design of efficient orange-red to red thermally activated delayed fluorescence emitters for OLEDs with external quantum efficiency of up to 26.0% and reduced efficiency roll-off. J Mater Chem C 2020;8(5):1614−22. https://doi.org/10.1039/C9TC05892C.

[38] Fan J, Miao J, Li N, Zeng Y, Ye C, Yin X, Yang C. A dual rigid donor and acceptor enabling red thermally activated delayed fluorescence emitters for efficient OLEDs with low efficiency roll-off. J Mater Chem C 2022;10(28):10255–61. https://doi.org/10.1039/D2TC02146C.

[39] Liu Y, Yang J, Mao Z, Ma D, Wang Y, Zhao J, Su SJ, Chi Z. Donor or acceptor:

molecular engineering based on dibenzo[a,c]phenazine backbone for highly efficient thermally-activated delayed fluorescence organic-emitting diodes. Adv Opt Mater 2023;11(1):2201695. https://doi.org/10.1002/adom.202201695.

[40] Xie W, Peng X, Li M, Qiu W, Li W, Gu Q, Jiao Y, Chen Z, Gan Y, Liu KK, Su S-J. Blocking the energy loss of dexter energy transfer in hyperfluorescence OLEDs via one-step phenyl-fluorene substitution of TADF assistant host. Adv Opt Mater 2022;10(17):2200665. https://doi.org/10.1002/adom.202200665.

[41] Wang YY, Zhang YL, Tong K, Ding L, Fan J, Liao LS. Highly efficient red thermally activated delayed fluorescence materials based on a cyano-containing planar acceptor. J Mater Chem C 2019;7(48):15301–7. https://doi.org/10.1039/C9TC05349B.

[42] Furue R, Matsuo K, Ashikari Y, Ooka H, Amanokura N, Yasuda T. Highly efficient red–orange delayed fluorescence emitters based on strong π-accepting dibenzophenazine and dibenzoquinoxaline cores: toward a rational pure-red OLED design. Adv Opt Mater 2018;6(5):1701147. https://doi.org/10.1002/adom.201701147.

[43] Data P, Pander P, Okazaki M, Takeda Y, Minakata S, Monkman AP. Dibenzo[a,j]phenazine-cored donor–acceptor–donor compounds as green-to-red/NIR thermally activated delayed fluorescence organic light emitters. Angew Chem Int Ed 2016;55(19):5739–44. https://doi.org/10.1002/anie.201600113.

[44] Okazaki M, Takeda Y, Data P, Pander P, Higginbotham H, Monkman AP, Minakata S. Chem Sci 2017;8(4):2677–86. https://doi.org/10.1039/C6SC04863C.

[45] Wang H, Zhao B, Ma P, Li Z, Wang X, Zhao C, Fan X, Tao L, Duan C, Zhang J, Han C, Chen G, Xu H. A red thermally activated delayed fluorescence emitter

employing dipyridophenazine with a gradient multi-inductive effect to improve radiation efficiency. J Mater Chem C 2019;7(25):7525–30. https://doi.org/10.1039/C9TC02557J.

[46] Zhao B, Wang H, Han C, Ma P, Li Z, Chang P, Xu H. Highly efficient deep-red non-doped diodes based on a T-shape thermally activated delayed fluorescence emitter. Angew Chem Int Ed 2020;59(43):19042–7. https://doi.org/10.1002/anie.202008885.

[47] Chen JX, Wang K, Zheng CJ, Zhang M, Shi YZ, Tao SL, Lin H, Liu W, Tao WW, Ou XM, Zhang XH. Red organic light-emitting diode with external quantum efficiency beyond 20% based on a novel thermally activated delayed fluorescence emitter. Adv Sci 2018;5(9):1800436. https://doi.org/10.1002/advs.201800436.

[48] Balijapalli U, Lee YT, Karunathilaka BSB, Tumen-Ulzii G, Auffray M, Tsuchiya Y, Nakanotani H, Adachi C. Tetrabenzo[a,c]phenazine backbone for highly efficient orange–red thermally activated delayed fluorescence with completely horizontal molecular orientation. Angew Chem Int Ed 2021;60(35):19364–73. https://doi.org/10.1002/anie.202106570.

[49] Wang YY, Tong KN, Zhang K, Lu CH, Chen X, Liang JX, Wang CK, Wu CC, Fung MK, Fan J. Positive impact of chromophore flexibility on the efficiency of red thermally activated delayed fluorescence materials. Mater Horiz 2021;8(4):1297–303. https://doi.org/10.1039/D1MH00028D.

[50] Qu C, Wang H, Man Y, Li Z, Ma P, Chang P, Li X, Han C, Pang Y, Xu H. Asymmetric intramolecular charge transfer enables highly efficient red thermally activated delayed fluorescent emitters. Chem Eng J 2023;457:141061. https://doi.org/10.1016/j.cej.2022.141061.

[51] Zhao T, Jiang S, Tao XD, Yang M, Meng L, Chen XL, Lu CZ. Dihydrophenazine-derived thermally activated delayed fluorescence emitters for highly efficient orange and red organic light-emitting diodes. Dyes Pigments 2023;211:111065. https://doi.org/10.1016/j.dyepig.2022.111065.

[52] Kothavale S, Kim SC, Cheong K, Zeng S, Wang Y, Lee JY. Solution-processed pure red TADF organic light-emitting diodes with high external quantum efficiency and saturated red emission color. Adv Mater 2023;35(13):2208602. https://doi.org/10.1002/adma.202208602.

[53] Wang S, Yan X, Cheng Z, Zhang H, Liu Y, Wang Y. Highly efficient near-infrared delayed fluorescence organic light emitting diodes using a phenanthrene-based charge-transfer compound. Angew Chem Int Ed 2015;54(44):13068–72. https://doi.org/10.1002/anie.201506687.

[54] Wang S, Cheng Z, Song X, Yan X, Ye K, Liu Y, Yang G, Wang Y. Highly efficient long-wavelength thermally activated delayed fluorescence OLEDs based on dicyanopyrazino phenanthrene derivatives. ACS Appl Mater Interfaces 2017;9(11):9892–901. https://doi.org/10.1021/acsami.6b14796.

[55] Liu Q, Chen WC, Zhang R, Wei H, Liu B, Jin JM, Liu Y, Ye Z, Chen JX, Ji S, Zhang HL, Huo Y. Design, synthesis, and electroluminescence of red TADF dyes based on cyanophenanthrene. Dyes Pigments 2023;212:111125. https://doi.org/10.1016/j.dyepig.2023.111125.

[56] Hu Y, Zhang Y, Han W, Li J, Pu X, Wu D, Bin Z, You J. Orange–red organic light emitting diodes with high efficiency and low efficiency roll-off: boosted by a fused acceptor composed of pyrazine and maleimide. Chem Eng J 2022;428:131186. https://doi.org/10.1016/j.cej.2021.131186.

[57] Yang T, Cheng Z, Li Z, Liang J, Xu Y, Li C, Wang Y. Improving the efficiency of

red thermally activated delayed fluorescence organic light-emitting diode by rational isomer engineering. Adv Funct Mater 2020;30(24):2002681. https://doi.org/10.1002/adfm.202002681.

[58] Xie W, Li M, Peng X, Qiu W, Gan Y, Chen Z, He Y, Li W, Liu K, Wang L, Gu Q, Su SJ. “On-off” switch between red thermally activated delayed fluorescence and conventional fluorescence by isomeric regulation. Chem Eng J 2021;425:131510. https://doi.org/10.1016/j.cej.2021.131510.

[59] Liu Y, Yang J, Mao Z, Wang Y, Zhao J, Su SJ, Chi Z. Isomeric thermally activated delayed fluorescence emitters for highly efficient organic light-emitting diodes. Chem Sci 2023;14(6):1551–6. https://doi.org/10.1039/D2SC06335B.

[60] Kukhta NA, Higginbotham HF, Matulaitis T, Danos A, Bismillah AN, Haase N, Etherington MK, Yufit DS, McGonigal PR, Gražulevičius JV, Monkman AP. Revealing resonance effects and intramolecular dipole interactions in the positional isomers of benzonitrile-core thermally activated delayed fluorescence materials. J Mater Chem C 2019;7(30):9184–94. https://doi.org/10.1039/C9TC02742D.

[61] Haykir G, Aydemir M, Tekin A, Tekin E, Danos A, Yuksel F, Hizal G, Monkman AP, Turksoy F. Effects of donor position and multiple charge transfer pathways in asymmetric pyridyl-sulfonyl TADF emitters. Mater Today Commun 2022;31:103550. https://doi.org/10.1016/j.mtcomm.2022.103550.

[62] Danos A, Gudeika D, Kukhta NA, Lygaitis R, Colella M, Higginbotham HF, Bismillah AN, McGonigal PR, Grazulevicius JV, Monkman AP. Not the sum of their parts: understanding multi-donor interactions in symmetric and asymmetric

TADF emitters. J Mater Chem C 2022;10(12):4737–47. https://doi.org/10.1039/D1TC04171A.

[63] Frisch MJ, Trucks GW, Schlegel HB, Scuseria GE, Robb MA, Cheeseman JR, Scalmani G, Barone V, Petersson GA, Nakatsuji H, Li X, Caricato M, Marenich AV, Bloino J, Janesko BG, Gomperts R, Mennucci B, Hratchian HP, Ortiz JV, Izmaylov AF, Sonnenberg JL, Williams-Young D, Ding F, Lipparini F, Egidi F, Goings J, Peng B, Petrone A, Henderson T, Ranasinghe D, Zakrzewski VG, Gao J, Rega N, Zheng G, Liang W, Hada M, Ehara M, Toyota K, Fukuda R, Hasegawa J, Ishida M, Nakajima T, Honda Y, Kitao O, Nakai H, Vreven T, Throssell K, Montgomery JA, Jr., Peralta JE, Ogliaro F, Bearpark MJ, Heyd JJ, Brothers EN, Kudin KN, Staroverov VN, Keith TA, Kobayashi R, Normand J, Raghavachari K, Rendell AP, Burant JC, Iyengar SS, Tomasi J, Cossi M, Millam JM, Klene M, Adamo C, Cammi R, Ochterski JW, Martin RL, Morokuma K, Farkas O, Foresman JB, Fox DJ. Gaussian 16 Rev A 03, Wallingford CT, 2016.

[64] Ni F, Huang C-W, Tang Y, Chen Z, Wu Y, Xia S, Cao X, Hsu J-H, Lee W-K, Zheng K, Huang Z, Wu C-C, Yang C. Integrating molecular rigidity and chirality into thermally activated delayed fluorescence emitters for highly efficient sky-blue and orange circularly polarized electroluminescence. Mater Horiz 2021;8(2):547–55. https://doi.org/10.1039/D0MH01521K.

[65] Liu B, Chen W-C, Zhang R, Liu Q, Wei H, Wu W-L, Xing L, Wang R, Liu Y, Ji S, Zhang H-L, Huo Y. Modulating optoelectronic properties of red TADF emitters based on acenaphtho[1,2-*b*]quinoxaline-3,4-dicarbonitrile through

isomeric engineering. Dyes Pigments 2023;216:111314. https://doi.org/10.1016/j.dyepig.2023.111314.

[66] Stavrou K, Danos A, Hama T, Hatakeyama T, Monkman A. Hot vibrational states in a high-performance multiple resonance emitter and the effect of excimer quenching on organic light-emitting diodes. ACS Appl Mater Interfaces 2021;13(7):8643–55. https://doi.org/10.1021/acsami.0c20619.

[67] Stavrou K, Franca LG, Monkman AP. Photophysics of TADF guest−host systems: introducing the idea of hosting potential. ACS Appl Electron Mater 2020;2(9):2868–81. https://doi.org/10.1021/acsaelm.0c00514.

[68] Chen J-X, Xiao Y-F, Wang K, Sun D, Fan X-C, Zhang X, Zhang M, Shi Y-Z, Yu J, Geng F-X, lee C-S, Zhang X-H. Managing locally excited and charge-transfer triplet states to facilitate up-conversion in red TADF emitters that are available for both vacuum- and solution-processes. Angew Chem Int Ed 2021;60(5):2478–84. https://doi.org/10.1002/anie.202012070.

[69] Samanta PK, Kim D, Coropceanu V, Brédas J-L. Up-conversion intersystem crossing rates in organic emitters for thermally activated delayed fluorescence: impact of the nature of singlet vs triplet excited states. J Am Chem Soc 2017;139(11):4042–51. https://doi.org/10.1021/jacs.6b12124.

[70] Franca LG, Danos A, Monkman A. Spiro donor – acceptor TADF emitters: naked TADF free from inhomogeneity caused by donor acceptor bridge bond disorder. Fast rISC and invariant photophysics in solid state hosts. J Mater Chem C 2022;10(4):1313–25. https://doi.org/10.1039/D1TC04484B.

[71] Hua L, Liu Y, Liu B, Zhao Z, Zhang L, Yan S, Ren Z. Constructing high-efficiency orange-red thermally activated delayed fluorescence emitters by three-dimension molecular engineering. Nat Commun 2022;13:7828.

https://doi.org/10.1038/s41467-022-35591-w.

[72] Yang W, Ning W, Jungchi H, Liu T, Yin X, Ye C, Gong S, Yang C. Polycyclic phenazine-derived rigid donors construct thermally activated delayed fluorescence emitters for highly efficient orange OLEDs with extremely low roll-off. Chem Eng J 2022;438:135571. https://doi.org/10.1016/j.cej.2022.135571.

[73] Zhao T, Jiang S, Wang Y, Hu J, Lin F-L, Meng L, Gao P, Chen X-L, Lu C-Z. Realizing high-efficiency orange-red thermally activated delayed fluorescence materials through the construction of intramolecular noncovalent interactions. ACS Appl Mater Interfaces 2023;15(25):30543–52. https://doi.org/10.1021/acsami.3c04117.

[74] Dias FB, Penfold TJ, Monkman AP. Photophysics of thermally activated delayed fluorescence molecules. Methods Appl Fluoresc 2017;5(1):012001. https://doi.org/10.1088/2050-6120/aa537e.

[75] Jankus V, Chiang CJ, Dias F, Monkman AP. Deep blue exciplex organic light-emitting diodes with enhanced efficiency; P-type or E-type triplet conversion to singlet excitons?. Adv Mater 2013;25(10):1455–9. https://doi.org/10.1002/adma.201203615.

[76] Cai X, Xu Y, Pan Y, Li L, Pu Y, Zhuang X, Li C, Wang Y. Solution-processable pure-red multiple resonance-induced thermally activated delayed fluorescence emitter for organic light-emitting diode with external quantum efficiency over 20%. Angew Chem Int Ed 2023;62(7):e202216473. https://doi.org/10.1002/anie.202216473.

[77] Zhang Q, Sun S, Liu W, Leng P, Lv X, Wang Y, Chen H, Ye S, Zhuang S, Wang L. Integrating TADF luminogens with AIE characteristics using a novel acridine – carbazole hybrid as donor for high-performance and low efficiency

814 roll-off OLEDs. J Mater Chem C 2019;7(31)9487–95.